Ifestos

Blue Bariagaber, Julia Ciesielska, Agapitos Dovles, Dorian Stefan Dumitru, Matteo Fonsetti, Louis Foujols, Lena Macke, Afonso Mota, Belen Lopez Pardo, Zoe Parlapani, Michał Pietras, Jacob Schimpl, Ignas Selevicius, Johanna Erna Charlotte Teuchert, Maria Abadia Varela

Tutors: Jörn Helbert and Günter Kargl

July 22, 2026

Abstract

Ifestos is a mission concept designed to investigate the Io-Jupiter system. Io is the most volcanically active body in the Solar System and the dominant plasma source of the Jovian magnetosphere, yet no mission has studied the complete sequence from volcanic supply through the exosphere to the plasma torus. Through repeated close flybys of Io, in-situ crossings of the plasma torus and global remote mapping, Ifestos will characterise Io's interior and volcanic activity, connecting it to the plasma and magnetic environment in the inner Jupiter system. With a comprehensive set of instruments and an orbit optimized for the science case, Ifestos will complement the ESA JUICE and NASA Europa Clipper and Juno missions, providing the first end-to-end view of the coupled Io–Jupiter system and establishing a benchmark for the study of mass-loaded magnetospheres and tidally heated planetary systems.

1. SCIENCE BACKGROUND

Jupiter's inner magnetosphere is driven by Jupiter's own internal plasma source, the innermost Galilean moon Io [1]. Io's close distance to Jupiter (5.9 R_J) drives strong periodic tidal deformation and continuous volcanism. Part of the gas that escapes during volcanic eruptions on Io is ionized by UV radiation and accumulated in the Io torus region [2]. This leads to the continuous supply of ions in Jupiter's magnetosphere [3], [4], [5]. Despite the fact that a large number of previous and ongoing missions have visited the Jovian system, many questions remain unanswered regarding the coupling processes between Io, the plasma torus, and the overall inner magnetosphere.

1.1. The Io-Jupiter System

While results from the Galileo mission indicated a global magma ocean [6] on Io, recent results from Juno seem to preclude a shallow global sub-surface magma ocean on Io, favouring a mostly solid mantle with partial melt [7]. The spatial distribution of this melt and its internal traits remain open [8].

Io's exosphere is dominated by SO_2 and sustained by constant volcanic supply. Its density and structure showcase high variability. Io's dayside exosphere composition and density have been analyzed in much more detail than the nightside counterpart, which according to models exhibits a different exospheric composition [1]. Approximately 1 ton/s of atmospheric material is accreted to the Jovian magnetosphere through escape processes, then ionized by UV radiation, charge exchange, and other processes. The relative importance of these mechanisms, and their response to volcanic variability, are not fully understood [1], [2], [4]. Ions and electrons undergo acceleration processes within the local magnetic environment and the resulting oxygen- and sulfur-rich plasma forms the dense plasma torus [2], [4]. The coupling processes between Io's volcanic activity and Jupiter's inner magnetosphere are yet to be fully understood. In order to unravel the role of the relevant physical mechanisms simultaneous measurements of the volcanic source, neutral environment, plasma properties and global torus state are required.

1.2. Io's Local Plasma Interaction and Ionosphere

The magnetized plasma surrounding Io rotates faster than the moon and interacts directly with its exosphere and ionosphere, as well as the surrounding magnetic environment. Several processes regulate how efficiently neutral material is converted into magnetospheric plasma [2], [4]. Galileo obtained six radio-occultation profiles in 1997, but all were acquired near the terminator and covered a limited range of illumination and plasma geometries. Since then, the ionosphere has not been systematically characterized as a function of longitude, local time, volcanic activity or upstream conditions [9].

1.3. Plasma Transport, Acceleration and Loss

After entering the torus, plasma is transported radially outward through Jupiter's magnetosphere over timescales of weeks. During this process, ion populations undergo acceleration and loss processes and shape the characteristic energetic spectra of Jupiter's intense radiation belts. These processes are not fully understood [3], [10], [11]. Particles are simultaneously removed through charge exchange with neutral gas, radial escape, precipitation, wave-driven pitch-angle scattering and absorption by Io or Europa [4], [5], [10], [12]. Distinguishing these mechanisms requires simultaneous measurements of particle energy and angular distributions, ion composition, electromagnetic wave activity, and neutral populations. Previous and ongoing missions have mostly focused on such mechanisms outside Europa's orbit [5], [13].

1.4. Current Observational Context and Scientific Opportunity

Several missions have provided important measurements of the Io–Jupiter system. However, none of these were designed to specifically study Io and its surrounding environment. Jupiter Icy Moons Explorer (JUICE) will provide a comprehensive investigation of the Jovian magnetosphere and the plasma environments of the icy moons. However, the mission's objectives are optimized for studying Europa, Callisto and Ganymede. In the context of this mission, Io and the inner magnetosphere will generally be observed remotely [11], [14]. Europa Clipper will focus on the Jovian plasma environment around Europa, and will not improve the understanding of Io significantly [15]. A dedicated Io mission would provide considerable scientific return by measuring Io's interior and volcanism, exosphere and ionosphere, particle escape, and plasma torus. This would additionally establish the Io-Jupiter system as an analogue for tidally-forced, magnetically-coupled systems beyond the Solar System [2], [16], [17].

1.5. Io as a laboratory for hot rocky exoplanets

Io is the only Solar System body where tidal heating, volcanism and the associated exosphere can be measured directly. The same processes are expected to govern rocky exoplanets orbiting close to their stars, where outgassing may sustain thin secondary atmospheres. Measurements at Io provide detailed information that exoplanet observations cannot supply [2], [7], [16], [17].

2. SCIENCE & MISSION CASE

The science and mission cases of IFESTOS, both here condensed for brevity, is centered on studying the Io-Jupiter system, particularly focusing on the high-energy processes governing Io, its material release, and the surrounding plasma torus and magnetic environment. This will be achieved through three complementary approaches: (1) repeated close flybys of Io will constrain its gravity field and tidal response, monitor volcanic activity, and measure its exosphere, ionosphere and neutral outflow; (2) repeated torus crossings will measure plasma composition, particle distributions, fields, waves and transport locally; and (3) global remote mapping of the torus and the surrounding magnetic environment. The strategy combines second-to-minute kinetic measurements with coverage of the approximately ten-hour Jovian rotation and repeated observations over at least 6 months [13]. The mission is complementary to JUICE and Europa Clipper, by characterising a key region of the Jupiter system which these missions will not [11], [14], [15]. In particular, it can provide plasma information on compsition and density variations which can be used to validate and improve the other mission's data. The Io–Jupiter system also offers a unique opportunity to study processes that cannot be spatially resolved in extrasolar systems.

2.1. Mission objectives

In order to achieve the mission goal, the following objectives (MO) were defined:

MO-1: Determine how Io supplies plasma to Jupiter's inner magnetosphere and how the resulting plasma torus is structured, transported, heated, accelerated and lost.

- Determine the three-dimensional structure and temporal evolution of the Io plasma torus.
- Identify the local kinetic processes that heat, accelerate, transport and remove Io-sourced plasma in Jupiter's inner magnetosphere.
- Quantify the ionisation, pickup and transfer of mass and energy from Io's exosphere and ionosphere into the plasma torus.

MO-2: Characterise the spatial and temporal dynamics of Jupiter's plasma boundaries and current sheets in the planets inner magnetosphere.

- Determine the structure and variability of plasma boundaries in the Io interaction region and inner magnetosphere.
- Search for and characterise signatures of magnetic reconnection and other non-ideal energy-conversion processes in the inner Jovian current sheet.

MO-3: Determine how Io's volcanic activity contributes to Io's exosphere and study Io's interior subsurface magma reservoirs.

- Constrain Io's interior structure, tidal deformation and spatial distribution of tidal heat dissipation.
- Characterise the spatial distribution and temporal variability of Io's volcanic activity.
- Characterise the composition, structure and temporal variability of Io's exosphere.

MO-4: Study what Io's tidal heating, exosphere, and torus can reveal on the interior state, volcanism, and mass loss in close-in exoplanetary systems.

- Quantify the relationship between Io's tidal response, surface heat-flow distribution and volcanic thermal output.
- Determine which unresolved ultraviolet and radio signatures trace mass loading, transport and loss in rotation-dominated plasma tori.
- Determine which exospheric signatures trace volcanic outgassing and escape from tidally heated rocky bodies.

2.2. Key requirements

To achieve the science objectives, several complementary measurements are planned. The global structure and composition of the Io plasma torus will be mapped remotely in the ultraviolet by the Ultra Violet Spectrograph (UVS) and in-situ by energetic neutral atom and ion imaging (ENAI), the energetic and the electron detectors (Electron detector (ED)). Acceleration and loss processes will be constrained by the magnetometers (MAG) and the radio and plasma wave instrument (RPW), complemented by electron density profiles from radio occultation Radio Science Experiment (RSE). The RSE will also be performed for gravity experiments during flybys. Io's surface and volcanism will be characterised through imaging with a Wide Angle Camera (WAC), and through spectrometry in the visible and near-infrared (VIRIS), as well as in the mid-infrared (Thermal Infrared Imager (TIRM)).

3. INSTRUMENTATION

3.1. Magnetometers (MAG)

On a 10.6 m boom two fluxgate magnetometers (FGM) (one close to the spacecraft, one in the middle) and a scalar magnetometer (at the tip) will be mounted. The FGM mounted closer to the spacecraft will detect disturbance by other instruments - which enables differentiating them from the environmental magnetic field. The scalar sensor is included to enable calibration of the FGM's measurements during phases when the magnetic field is highly variable so that typical techniques do not work work [18]. The magnetometer for this mission is based on Juno's MAG [19]. The instruments will cover a dynamic range up to 150×10^3 nT with a resolution of 0.05 nT per vector component.

3.2. ENAI

The ENAI is based on JUICE's PEP-JENI and Juno's JEDI [20]. A set of three ENAIs will be mounted on the spacecraft in a way that ensures almost full sky coverage, while one of them will be nadir-facing towards Jupiter. The ENAI has two modes: ENA imaging and ion imaging. Outside the plasma torus, the nadir-facing ENAI will be in ENA imaging mode to observe Jupiter, while the other two are turned off. In the torus, all three ENAIs will be in ion imaging mode to provide enough data to reconstruct the full phase space distribution [20]. Compared to JENI, the entrance voltage was increased and a still voltage was added to filter out low-energy ions. The measurable energy range is 0.5 keV to 300 keV for ENAs and 0.5 keV to 5 MeV for ions with a resolution of $\Delta E/E \ \leq 30\ \%$ This resolution is sufficient to resolve hydrogen, helium, oxygen and sulfur ions [21].

3.3. RPW

The Radio and Plasma Wave instrument (RPW) is based on JUICE-RPWI [22]. It comprises 4 Langmuir probes (LP), each one on a 3 m boom in a tetrahedral configuration, a triaxial search coil magnetometer (SCM) and a high frequency antenna (HF) on the magnetometer boom, and an electronics box (EBOX) inside the shielded vault. The LPs measure electric field fluctuations from 1 Hz to 2 MHz and the SCM measures magnetic fluctuations from 1 Hz to 150 kHz, while the HF receiver sounds the plasma frequency from 1 Hz to 45 MHz, giving an independent calibration of the LPs. Cold-plasma moments are returned at 1 s cadence and survey spectra every 1–10 s, with burst waveforms at up to 4M samples/s during Io flybys and torus crossings. By varying the voltage at the probes, they can provide information on local plasma density and temperature.

3.4. ED

The Electron Detector (ED) is an adapted version of the PEP-JoEE electron spectrometer from the JUICE mission. It will be capable of detecting electrons in an energy range of 28 keV/q to 2MeV/q with an energy resolution of $\Delta E/E = 20\%$ [20], and is therefore well equipped for the Io plasma environment [1]. The FOV is $12° \times 180°$, which is why three EDs facing in the same three different directions as the ENAIs will be used to reconstruct the 3D phase space distribution. The instruments will detect electrons based on an anti-coincidence between valid events and background events and a matching-energy coincidence segment [23].

3.5. UVS

The Ultraviolet Spectrograph (UVS) is an ultraviolet spectrograph adapted from JUICE-UVS [24], designed to map the Io plasma torus in the Extreme Ultra-Violet (EUV) and FUV. It covers a contiguous bandpass of 60-140 nm at a spectral resolution of 0.5 nm FWHM, slightly lower than that of the heritage JUICE instrument. This allows separation of the S IV (74.8 nm) and S II (76.5 nm) lines whose ratio tracks compositional change, along with S III (68.0 nm), O II (83.3 nm) and the O I doublet at 130.4 and 135.6 nm. A 7.5° slit with a resolution of 0.16° is stepped by a two-axis scan mechanism building a complete map of the torus (5–10 R_J radially and $\pm 2R_J$ vertically) every 20 minutes. The line intensities and their ratios yield the ionic composition, charge states, electron temperature and column density of the torus.

3.6. Radio Science Experiment (RSE)

The RSE will use the spacecraft–Earth radio link as a scientific measurement system. It will perform two complementary investigations: close-flyby Doppler measurements of inhomogenities in Io's gravitational field to constrain its interior and tidal response, and radio-occultation measurements to characterise its exosphere and surrounding plasma environment [7]. A KaT transponder provides the coherent two-way Ka/Ka link used for precision Doppler measurements [25]. A high-precision Ultra Stable Oscillator (USO), based on a quartz resonator with double oven technology, provides the highly stable onboard reference required for one-way X/Ka radio occultations [26].

3.7. Visual and near InfraRed Imaging Spectrometer (VIRIS)

VIRIS covers the spectral range from 0.5–5.5 μm bands with a spatial resolution of 75 m/pixel at 500 km distance from Io, and a 3.4° FOV. It maps the composition and thermal emission of the surface and exosphere of Io, focusing on volcanic deposits. [27], [28].

3.8. TIRM

TIRM is a high-spatial-resolution thermal infrared mapper derived from IVO's TMAP and BepiColombo's MERTIS. It combines an uncooled microbolometer array with two radiometer line detectors. The bolometer uses 8 filters from 2 to 16 μm to derive the surface composition of Io at a spatial resolution of 625 m/pixel at 500 km distance. The radiometer covers the wavelength range from 8 to 40 μm for precise surface temperature measurements at a spatial resolution of 9.4 km/pixel at 500 km distance [29].

3.9. WAC

The WAC is a NUV to NIR imager developed for IVO based on the WAC for the Lunar Reconnaissance Orbiter. It will take close up images of Io with an expected resolution of 108 m/pixel at 500 km distance. The required pointing is set at 41 arcsec. With the WAC we expect to cover approximately 4 % of Io's surface per fly-by [30].

3.10. Radiation Monitor (RADMON)

The is a detector for high-energy electrons, protons and heavy ions adapted from JUICE's RADEM [31]. It constantly monitors the energy spectra and direction-resolved fluxes of charged particles not only in orbit around Jupiter but also during all other mission phases to monitor the radiation. Its data is also used for housekeeping. The detectable particle energies are 0.3 MeV to 40 MeV for electrons and 5 MeV to 250 MeV for protons.

4. MISSION ANALYSIS

4.1. Mission Phases and Key Drivers

The mission is driven by:

- **Radiation environment and observation**: the target science orbit's periapsis lies within the Io plasma torus, the most intense region of the Jovian radiation belts. The mission also needs to survey the plasma torus from a polar vantage minimum distance of 13 Jupiter radii (R_J).
- **Long transfer and tour duration**: 7 years transfer plus an estimated 2.5 years for the post-insertion moon tour.
- **Power and eclipse constraints**: Constant sight of the Sun to provide power throughout mission lifetime.
- **Communication windows**: At least two 8h communication window per Jovian orbit to return scientific findings.

The envisioned mission timeline includes the following phases: launch, interplanetary transfer, Jupiter orbit insertion, Jovian tour, science orbit (nominal and possible extended mission), and end-of-life disposal.

4.2. Transfer to Jupiter

The transit to Jupiter was first analysed through Tisserand plots, which identified the Earth–Venus–Earth–Earth–Jupiter (EVEEJ) sequence as the favourable transfer option. Subsequent analysis using TudatPy [32] determined the phasing and velocity at each node, yielding the transfer sequence presented in Table 2.

Event	Date
Launch	13/10/2037
Venus Flyby	17/03/2038
Earth Flyby	04/01/2039
Earth Flyby	03/01/2041
Jupiter Arrival	20/09/2044

Table 1. Timeline of transit to Jupiter

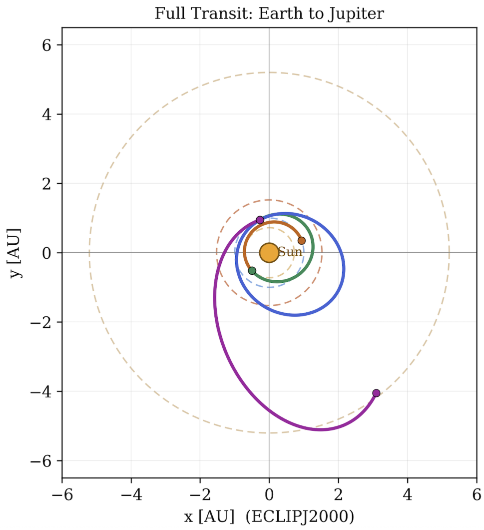

Figure 1. EVEEJ Flyby Sequence

The launch is performed from Ariane 64, with a characteristic energy of $C_3 = 11.28$ km^{2}s^{-2}. The transfer employs ArianeGroup S400-15 Bipropellant propulsion system, with a total transfer Δv of 4.6 km/s and a total minimum time of flight of 9.5 years. A bilinear interpolation of the Ariane 64 performance data for the specific trajectory sets a maximum launch capacity of 5626.2 kg, confirming mission feasibility with a tight mass margin of 63.75 kg (1.15 %).

4.3. Insertion

For the final leg of the transfer (Earth–Jupiter), a B-plane targeting strategy is planned to achieve the desired orbital inclination of 80°. The incoming hyperbolic trajectory targets Io, establishing at insertion the periapsis radius that is maintained throughout the subsequent tour phase [30]. The resulting insertion semi-major axis is $\approx 5.44 \times 10^{10}$ km with a required burn of 693.18 m/s, applied at perikrone.

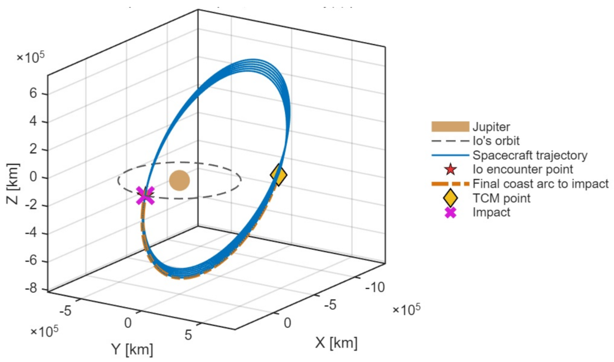

Figure 2. Ifestos orbit around Jupiter

4.4. Jovian Tour

The interval between Jupiter arrival and insertion into the target orbit represents the least well-constrained segment of the trajectory. To reduce the apoapsis to its target value, a moon-tour strategy employing a sequence of gravity-assist flybys of Ganymede and Callisto is planned, following the precedent established by the Galileo mission [33]. Based on this precedent, the apoapsis is estimated to reduce the target value to 1.3×10^6 km within approximately 2 years [33].

4.5. Science Orbit

Once the target orbit is achieved, the spacecraft will perform flybys of Io at altitudes below 500 km and maintain this orbit for a duration of at least six months. Selection of the orbit was carried out through analysis of the orbital resonance between the spacecraft and Io. Three constraints governed this selection: (i) a z-coordinate (out-of-plane distance along the polar axis) of at least 13 Jupiter radii, to enable observation of the jovian system from directly above the pole; (ii) a periapsis coincident with Io's orbital distance, to allow for flybys at altitudes below 500 km; and (iii) an orientation of the orbital line of nodes perpendicular to the Jupiter–Sun vector, to maintain uninterrupted solar illumination of the spacecraft. These constraints together define a resonant orbit with an apoapsis radius of 18.6 R_J, illustrated in Figure 2.

The orbital period of the science orbit is 5.3 days. Radiation exposure during the six-month science phase is estimated using SPENVIS (see section 5.1). Due to constraint (iii) listed previously, there are no periods of eclipse. This orbital configuration also preserves communication links throughout the mission lifetime around Jupiter, maintaining an Earth-Probe-Sun angle greater than European Space Agency (ESA)'s baseline recommendation of 3° [34].

4.6. End Of Life (EOL)

The EOL disposal strategy is impact with Io's surface, in accordance with ESA's Planetary Protection Policy [35]. A Δv of 0.69 m/s applied at the apokrone targets impact with Io, requiring approximately 2.5 days to complete the deorbit sequence.

4.7. Delta-V Budget

Event	Days Elapsed	Δv [m/s]
Launch	0	3360.480
Venus Flyby	157.8	1.106
Earth Flyby	450.1	0.059
Earth Flyby	1180.6	0.940
Jupiter Arrival	2536.7	693.181
Jovian System	$\approx$730	500
End of Life	-	0.69

Table 2. Timeline of transit to Jupiter

5. SPACECRAFT

The design of the Ifestos satellite bus is adapted from ESA's JUICE mission, with multiple subsystems having the same components and architecture. This is considered as an advantage, as the majority of the components, along with the structure of the bus, have already undergone development, testing, and deployment thus making the mission less costly. The S/C stowed for launch has dimensions of 4.09 x 2.86 x 4.35 m (X x Y x Z), while the S/C deployed in orbit measures 16.8 x 27.1 x 13.7 m. Visual representation of Ifestos spacecraft's preliminary design is shown in Figure 3.

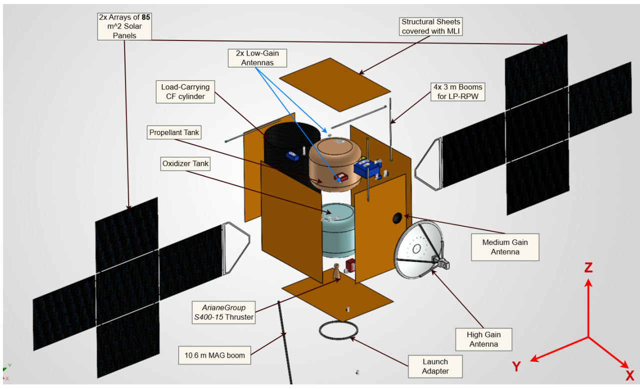

Figure 3. Ifestos spacecraft preliminary design

Wet and dry mass of the spacecraft is 5573.5 kg and 2866.2 kg, respectively. As per ESA margin philosophy, a 20% and 15% margins have been added to account for the subsystems margins and radiation shielding [36]. The complete mass budget can be seen in Table 3.

Subsystem	Mass incl. DMM [kg]
SSTC	360.0
Harness and Screws	215.7
AOCS	101.2
PROPSYS (tanks and thrusters)	197.7
EPS	690.2
Communications	94.6
OBC and PDH	25.9
PL (incl. margin)	296.0
Launch Adapter	95.00
Nominal Dry Mass at Launch	2076.92
Total Dry Mass at Launch	2492.3
Total Shielded Dry Mass at Launch	2866.1
Propellant	2646.8
Pressurizer	7.4
Total Propellant Mass	2707.3
Launch Mass	5573.5

Table 3. Ifestos Spacecraft Mass Budget

5.1. Structure, Shielding and Thermal Control

The spacecraft architecture is built around a load-bearing central cylinder which houses the propellant tanks. The structure is designed to comply with all instrument and subsystem pointing requirements. Microvibration effects induced by solar array deployments and orbital maneuvers have been taken into consideration. To protect sensitive electronics from the high-radiation environment, two shielded vaults are integrated along the central cylinder, while individual instruments incorporate supplementary shielding as required.

The radiation environment was modelled with SPENVIS, computing the total ionising dose accumulated over 6 months in Jovian orbit as a function of aluminium shielding thickness. The dose varies from 416 krad with 10 mm Al to 107 krad with 30 mm Al. The mission baseline is a global aluminium shielding of the spacecraft body, complemented by shielding incorporated into the housings of the individual instruments. The goal is to achieve a radiation dose of 150 krad or less on component level, based on the radiation hardness of the components. Where needed, local spot shielding with tantalum/titanium plates is added for the most susceptible units. Also, this multi-layered high-Z/low-Z graded shielding is accounting for secondary radiation emerging when high energetic particles are decelerated. The sizing and location of this additional local shielding will be based on a detailed particle ray tracing in a later mission phase. Solar cells use at least 300 µm coverglass with an ITO coating against displacement damage following the JUICE approach, and the RADMON instrument monitors the accumulated dose in flight.

The thermal control must evaluate two situations: the hot case in Venus flyby phase and the cold case, for entering Jupiter orbits. For the Venus flyby, the spacecraft pointing is optimized by using the HGA as a sunshield and tilting the solar arrays. On the other hand, the cold effects are mitigated by heaters and MLI and Black kapton.

5.2. AOCS

The Ifestos (AOCS) must maintain 3-axis attitude stabilization with a pointing stability of less than 41 arcsec. Additionally, the AOCS must sustain this pointing accuracy throughout the duration of the Wide Angle Camera (WAC) exposure time, as this instrument is determined to be the driver of the system . To satisfy these constraints, the following hardware combination was selected: two sun sensors, two Inertial Measurement Units (Inertial Measurement Unit (IMU)s), one triple-head star tracker, and four reaction wheels. The sun sensors, IMUs, and star tracker determine the attitude, while the reaction wheels execute attitude control and the thrusters manage reaction wheel desaturation. The *Sodern Hydra* star tracker has a high-frequency spatial error of 27 arcsec in the Z-axis. The actual pointing accuracy is further improved by an Extended Kalman Filter (EKF) that fuses data from the three orthogonally placed heads with IMU measurements, mathematically overriding weak Z-axis accuracy with strong X/Y data to safely satisfy the 41 arcsec pointing requirement. The majority of the selected components leverage JUICE heritage, but due to the necessity for a higher degree of radiation protection, all components are classified at TRL 6 for this mission.

5.3. Propulsion

The propulsion subsystem provides the capability required for trajectory correction manoueuvres during the interplanetary - Jovian phases, JOI and Final Orbit Insertion. It also covers functions associated with spacecraft attitude control and momentum management. The baseline configuration is based on a single ArianeGroup S400-15 main engine applied also in the JUICE Spacecraft, delivering 425 N of thrust, I sp of approximately 321 s and operating on a bipropellant hypergolic MMH + MON-3 combination. The selected thrust level resulted from an iterative propulsion sizing and trade off process considering JOI burn duration, propellant demand, propulsion system dry mass and the feasibility of a finite duration insertion manoeuvre. For the JOI design requirement of 807.99 m/s and the approximately 500 m/s for the final orbit insertion, the estimated main engine total firing duration is approximately 220,5 minutes. A critical system constraint during these prolonged main engine firings is the dynamic interaction between the propulsion system and the solar arrays. Sudden engine start-up or shut-down could induce structural oscillations. To mitigate this, the propulsion subsystem is commanded via a synchronized firing algorithm. This involves executing a calibrated pulse-and-gap sequence immediately prior to steady-state continuous firing, and a similar sequence at shut-down, allowing the solar arrays to reach equilibrium and stabilizing propellant fluid dynamics[28]. Attitude control during main engine operation, small trajectory corrections and reaction wheel momentum unloading are provided by sixteen S25 thrusters 23 N each, arranged 12 operational and 4 redundant units. The mass budget is 998.8 kg of MMH and 1648.0 kg of MON-3. It provides a nominal oxidiser to fuel mixture ratio of 1.65. The pressurisation system uses approximately 7.4 kg of helium, approximately 182 litres.

5.4. Electrical Power System

The subsystems of the spacecraft are powered by a solar array and batteries. In case of an eclipse or loss of attitude control the battery is sized for the spacecraft to survive seven hours in safe mode with a 40% margin. Due to varying power demands two operation modes are considered, peak power generation and nominal power generation.The dimensioning of the solar arrays is included in Table 4, including power margins.

	Peak Power with Margins	Nominal Power with Margins
Maximum EOL Power (W)	1075	892
Solar array area (m^2)	110	88
Battery capacity (kWh)	4	4

Table 4. Solar array and battery sizing for different power generation scenarios. The power generation can be controlled by rotating the solar panels.

Several options for sizing of solar arrays and battery were considered, ultimately the solar array surface was decreased to 95 m^2 and the batter power was increased to 5kWh, reducing the dependency on solar power.

In the sizing of the solar arrays their degradation over time was taken into account therefore insuring that the power generation will continuously stay above the threshold limit of 700 W until EOL. The power generation can be controlled by rotating the solar panels following the JUICE approach.

5.5. Power Budgeting for SciOps Modes

The total power consumption for each operational mode was calculated step-by-step by assessing the individual requirements of all subsystems and payloads, partially inspired by the JUICE mission's architecture.

Unit	SciOps High $[W]$	SciOps Normal $[W]$	SciOps Low + Coms $[W]$
Payload Io sensing	96.2	40.2	40.2
Payload In situ	76.5	53.3	9.7
Payload left	5.1	14	14
EPS	66	66	66
OBC	90.5	70	90.5
AOCS	134.4	134.4	134.4
COMS	72.4	17	72.4
Thermal	104.5	242.0	242.0
TOTAL	645.6	636.9	669.1

Table 5. Power budget for Science Operations modes

5.6. Command and Data Handling

There are two main parts: the OBC and the Solid-State Mass Memory (SSMM). The OBC is responsible of running the flight software: the processing of commands via the X and Ka bands, managing autonomous operations and interfacing with the rest of subsystems. On the other hand, the SSMM stores the critical science data until the next downlink window is available.

Due to the high-radiation environment, the main driving requirement, the following radiation-hardened components have been selected: Next Generation OBC and DSI data handling unit for SSMM. Moreover, the flight software incorporates EDAC (error detection and correction) protocols, to reduce the quantity of SEU (single event upsets). The design includes two fully redundant OBCs and two fully redundant SSMMs, to switch in case of failure. For the flyby critical stages, where data loss compromises the mission, the system operates under hot redundancy; for the rest of the mission, cold redundancy is implemented. To minimize the effects of radiation in science data, the data is stored thrice. The total size of each SSMM is of 1TBit, exceeding the requirement of 0.03 Tbit maximum uncompressed data, including margins, as shown in table 6. This would prevent data losses even if downlink windows are unavailable for several orbits. The maximum data obtained is due to the cameras: as the spacecraft only gets close enough to Io in certain orbits, those measurements are only taken during that period.

Total data per orbit	Uncompressed	Compressed
Average (Gbit)	5	2.75
Maximum (Gbit)	9.51	4.02

Table 6. Data budget

5.7. Telemetry, Tracking, and Command

This subsystem is responsible of receiving command signals and downlinking the mission data to the ground using the ESA ESTRACK network. It is composed of a Deep Space Transponder, a Traveling Wave Tube Amplifiers, a Radio Frequency Distribution Assembly, and four antennas. The procedure is as follows: it receives the compressed data buffer from the OBC, it generates the signal, it amplifies the signal and, finally, transmits it to the ground station; in addition, it receives telecommands. There are two frequencies available that work in parallel: the X-band is used for telecommands and housekeeping, while the Ka band is used for high-speed transmission of science data. X-band might be used as well for science data during adverse atmospheric conditions.

The antennae are of three different types: a high gain antenna, a medium gain antenna and two low gain antennae. The high gain antenna is a 2.5-meter diameter X/Ka-band antenna for communications in Jupiter. It is used for Ka and X bands downlink and X band uplink. The medium gain antenna is a 0.5-meter diameter X/Ka band antenna for cruise communications, and also to serve as backup if necessary. The low gain antennae are two omnidirectional antennas for communications close to Earth for X-band.

The primary driver of the design is the data bulk that needs to be transmitted to the ground. The link budget, for both Ka-band (science data) and X-band (science data plus housekeeping data) is included in table 7. The average orbit only has two communications windows (2.88 Gbits), which is enough for the average compressed data; for the orbits with maximum data produced, three communications windows (8 hour separate slots) are employed so the total data that can be downlinked (4.32 Gbits) exceeds the maximum data shown in Table 6.

Parameter	Ka band	X band
Average distance (km)	7.78E+08	7.78E+08
Transmitting Antenna Gain (dBi)	48.7	44.7
G/T (dB/K)	60	52.5
Data rate (kbps)	50	50
FSPL (dB)	300	287
Margin (dB)	1.1	1.9
Power (dBW)	10.5	14.4
Comms window duration (h)	8	8
Total data downlinked per window (GBit)	1.44	1.44

Table 7. Link budget for X and Ka bands

5.8. Payload

The payload subsystem consists of 10 unique instruments which are necessary to fulfill mission's scientific objectives. The placement of the instruments is driven by their individual observation and accommodation requirements and is shown in Figure 4. +Z axis of the bus is nadir (Io) pointing while

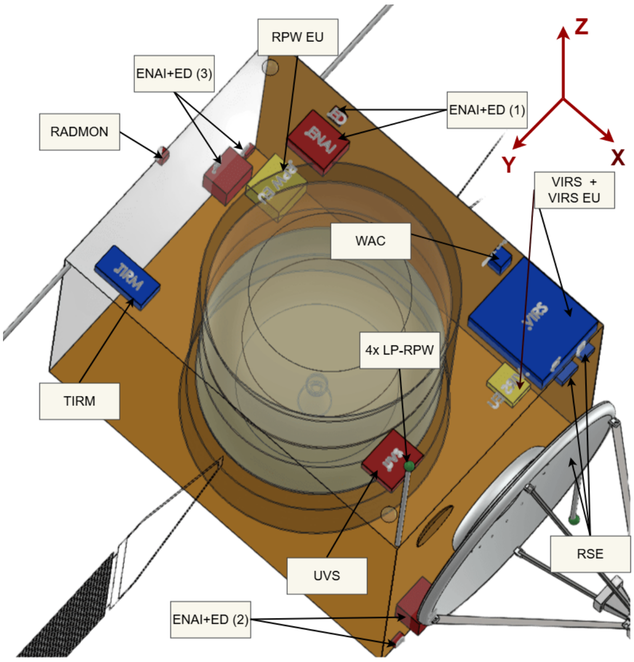

Figure 4. Ifestos instrument placement

-X represents ram pointing. The EUV imaging spectrometer (UVS), VIS imaging spectrometer (VIRIS), Wide Angle Camera (WAC), Thermal IR Imager (TIRM) are all placed on the nadir (Io) pointing side for torus (UVS) and Io imaging (VIRIS, WAC, TIRM). The Energetic Neutral Atoms and Ions Imager (ENAI) and Electron Detector (ED) are placed in pairs on three orthogonal sides of the bus to enable omnidirectional mapping of neutral atoms (outside the torus), and ions and electrons (inside the torus). The Radiation Monitor () is placed on ram pointing for housekeeping radiation monitoring. The Magnetometers (MAG) and Radio and Plasma Wave Instrument (RPW) instruments are placed on a 10.6-meter length Magnetic Boom to meet the magnetic cleanliness requirements necessary for scientific goals. The Langmuir Probes (LP-RPW) are placed on four shorter booms.

6. OPERATIONS

6.1. Spacecraft Modes

7 different spacecraft modes are implemented: LEOP Mode, Standby Mode, Commissioning Mode, Manoeuvre Mode, Safe Mode (with both Safe and Survival States), EOL Mode. The Science Operations Mode is divided in 3 states: High Power State for both flybys and closest approaches, Nominal Power State for routine campaigns and Low Power State including Downlinking process. All these modes require a nominal power ranging from 324W to 669W.

6.2. Technical Mission Schedule

The mission schedule is divided in three parts: project design and development, launch and cruise; and Jupiter orbit. The project design includes the following phases:

- Phase 0 (Q1 2028): mission preliminary analysis
- Phase A (Q1 2029: mission definition
- Phase B (Q1 2030): preliminary design
- Phase C (Q1 2032): critical design
- Phase D (2032-37): Instrument/ Platform development /verification

After that point, phase E starts and lasts from Q3 2037 to Q2 2043, with the insertion into the orbit. It covers launch and interplanetary travel, and it requires health checks every six months.
After the arrival to the Jovian systems, phase F or science operations begin, and they finish in Q1 2045; up from there, the spacecraft will keep on operating until EOL. After that point, disposal begins, crashing the satellite into Io.

6.3. Risk management

The risks evaluated for the mission are compiled in table 8, where PS stands for probability and IR for impact: total risk is a product of both. For the radiation exposure, mitigation includes shielding for components which cannot be redundant and for redundant components as well, annealation process and switch to second satellite bus; to spend time outside radiation belts; and also to reduce mission lifetime. For launch delays, the proposed strategy is multiple transfer orbits planned; for both components unavailability and long-lead time the plan includes early development and multiple component selection. Finally, early developments and margins will keep the mission within budget.

Description of risk	Description of impact	PS	IR	RISK
Radiation exposure	Destruction or malfunction of electronics and sensors	5	5	25
Launch gets delayed	Launch window closes so transfer gets impossible or dV heavy	2	5	10
Unavailability of components	Delay of project	3	3	9
Long-lead time components	Delay of project	3	3	9
Spent budget exceeds proposed budget	Descope science	3	3	9

Table 8. Risk Assessment Matrix

7. COST

The total estimated cost of the mission is 1000.8 million euros; the cost breakdown is shown in table 9.

Item	Price [MIO EUR]
Hardware payload and instruments Hardware platform	20 200
Platform engineering ESA project management (25% of all the above mentioned)	250 117.5
Mission operations Spacecraft operations	74 60
Launcher	135
TOTAL	**721.5**
TOTAL with 20% margin	**1000.8**

Table 9. Mission budget

Acronyms

AOCS Attitude and Orbit Control System. 6, 7

ED Electron detector. 3, 9
ENAI energetic neutral atom and ion imaging. 3, 9
EOL End Of Life. 6, 7, 9
ESA European Space Agency. 5, 6, 10
EUV Extreme Ultra-Violet. 4, 9

IMU Inertial Measurement Unit. 7

JUICE Jupiter Icy Moons Explorer. 2–4, 6–8

OBC On-Board Computer. 6, 8

RADMON Radiation Monitor. 4, 6
RPW radio and plasma wave instrument. 3, 9

RSE Radio Science Experiment. 3, 4

SSMM Solid-State Mass Memory. 8

TIRM Thermal Infrared Imager. 3, 4, 9

UVS Ultra Violet Spectrograph. 3, 4, 9

VIRIS Visual and near InfraRed Imaging Spectrometer. 4, 9

WAC Wide Angle Camera. 3, 4, 7, 9

8. REFERENCES

[1] F. Bagenal et al. (2020). *Journal of Geophysical Research: Space Physics, 125, e2019JA027485*.
[2] N. Thomas (2021). *Exp. Astron.*, vol. 54, no. 2-3, 791–807.
[3] E. Roussos et al. (2022). *Exp. Astron.*, vol. 54, 745–789.
[4] L. Roth et al. (2025). *Space Sci. Rev.*, vol. 221, no. 1, 13.
[5] M. Long et al. (2022). *J. Geophys. Res. Planets*, vol. 127, no. 4.
[6] K. K. Khurana et al. (2011). *Science*, vol. 332, no. 6034, 1186.
[7] R. S. Park et al. (2025). *Nature*, vol. 638, 69–73.
[8] C. W. Hamilton et al. (2013). *Earth and Planetary Science Letters*, vol. 361, 272–286.
[9] D. P. Hinson et al. (1998). *J. Geophys. Res. Space Phys.*, vol. 103, no. A12.
[10] N. Achilleos et al. (2015). *Space Sci. Rev.*, vol. 187, no. 1–4, 229–299.
[11] A. Masters et al. (2025). *Space Sci. Rev.*, vol. 221, no. 24.
[12] M. Long et al. (2025). *Nat. Commun.*, vol. 16, 7916.
[13] A. J. Steffl et al. (2007). *Icarus*, vol. 194, no. 1, 153–165.
[14] T. Denk et al. (2026). *Space Sci. Rev.*, vol. 222, 27.
[15] R. T. Pappalardo et al. (2024). *Space Sci. Rev.*, vol. 220, 40.
[16] J. Saur et al. (2013). *Astron. Astrophys.*, vol. 552, 20.
[17] C. W. Hamilton et al. (2025). *Planet. Sci. J.*, vol. 6, no. 6, 134.
[18] P. Brown et al. (2024). *EGU General Assembly 2024*.
[19] J. Connerney et al. (2017). *Space Sci Rev 213, 39–138*.
[20] S. Barabash et al. (2016).
[21] D. G. Mitchell et al. (2016). *Journal of Geophysical Research: Space Physics, Vol. 121, Issue 21*.
[22] J. Wahlund et al. (2021). *Space Sci Rev 221, 1*.
[23] S. Barabash et al. (2015). *EPSC Abstracts Vol. 10, EPSC2015-589, 2015 European Planetary Science Congress 2015*.
[24] M. W. Davis et al. (2021). *International Conference on Space Optics — ICSO 2020*, vol. 11852, 919–929.
[25] P. Cappuccio et al. (2025). *Aerospace*, vol. 12, no. 1, 56.
[26] A. Shapira et al. (2016). *2016 European Frequency and Time Forum (EFTF)*, 1–5.
[27] JUICE Science Working Team (2014). ESA/SRE(2014)1.
[28] G. Sarri et al. (2026). *Space Science Reviews*.
[29] J. Helbert et al. (2022). *Infrared Remote Sensing and Instrumentation XXX*, vol. 12233.
[30] E. Adams et al. (2012). *2012 IEEE Aerospace Conference*, 1–13.
[31] G. P. P. M. e. a. Hajdas W. (2025). *Space Sci Rev 221, 43 (2025)*.
[32] D. Dirkx et al. (2022). *Europlanet Science Congress*, vol. 16.
[33] L. A. D'Amario et al. (1992). *Space Science Reviews*, vol. 60, no. 1–4, 23–78.
[34] ECSS (2024).
[35] COSPAR (2021).
[36] SRE-PA and D-TEC staff (2012). SRE-PA/2011.097/.